Article

Bending and Torsional Stresses in Hypotrochoidal H-Profiled Shafts Standardised According to DIN 3689-1

Masoud Ziaei

Department of Mechanical and Automotive Engineering, Institute for Machin Development, Westsächsische Hochschule Zwickau, D-08056 Zwickau, Germany, masoud.ziaei@fh-zwickau.de

Abstract: Hypotrochoidal profile contours have been produced in industrial applications in recent years using twin-spindle processes, and they are considered effective high-quality solutions for positive shaft–hub connections. This study mainly concerns analytical approaches to determine the bending stresses in hypotrochoidal profile shafts. The formulation was developed according to bending principles using the mathematical theory of elasticity and conformal mappings. The loading was further used to investigate the rotating bending behaviour. The stress factors for the classical calculation of maximum bending stresses were also determined for all those profiles presented and compiled in the German standard DIN3689-1 for practical applications. The results were also compared with the corresponding numerical and experimental results, and very good agreement was observed. Additionally, based on previous work, the stress factor was determined for the case of torsional loading to calculate the maximum torsional stresses in the standardised profiles, and the results are listed in a table. This study contributes to the further refinement of the current DIN3689 standard.

Keywords: hypotrochoidal profile shafts; DIN3689 H-profiles; bending stress; rotating bending loads; flexure; torsional stress in profiled shafts; stress factor

1. Introduction

A significant advantage of hypotrochoidal profiles (H-profiles) is their manufacturability through two-spindle turning [1] and oscillating–turning [2] processes, as well as roller milling [3], which enable very time-efficient production. A new DIN sheet DIN3689-1 [4] was published involving the geometric properties of H-profiles for industrial applications.

In [5], the authors discussed torsion-loaded H-profiles in detail and determined torsional deformations for the standardised profiles. In another study, suitable conformal maps were presented, in which the first obtained values were used in successive methods [6], and torsional loading for H-sections was solved based on the method presented in [7].

To solve M-profiles (hybrid trochoids) subject to bending stresses, in [8], the authors used an analytical approach to study contour maps. This made it possible to derive exact solutions for the stresses and deformations in the M-profiles.

In the present work, the method in [8] was extended to hypotrochoidal profiles. The stress factors for the calculation of bending stresses in the H-profiles standardised according to DIN3689-1 were determined and compiled in a table. In addition, the corresponding stress factors for torsional loading were also calculated based on [5], the results of which are also listed in the table.

2. Geometry of H-profiles

A hypotrochoid (H-profile) is created by rolling a circular profile (called a rolling circle) on the inside of a guiding circle without slip (see, e.g., [9]). The distance between the centre point of the rolling circle and the generating point P is defined as eccentricity

Preprints (www.preprints.org) | NOT PEER-REVIEWED | Posted: 16 December 2022 doi:10.20944/preprints202212.0289.v1

(Figure 1). Depending on the diameter ratios of the two circles and the location of the generating point P in the rolling circle, different H-profiles are formed.

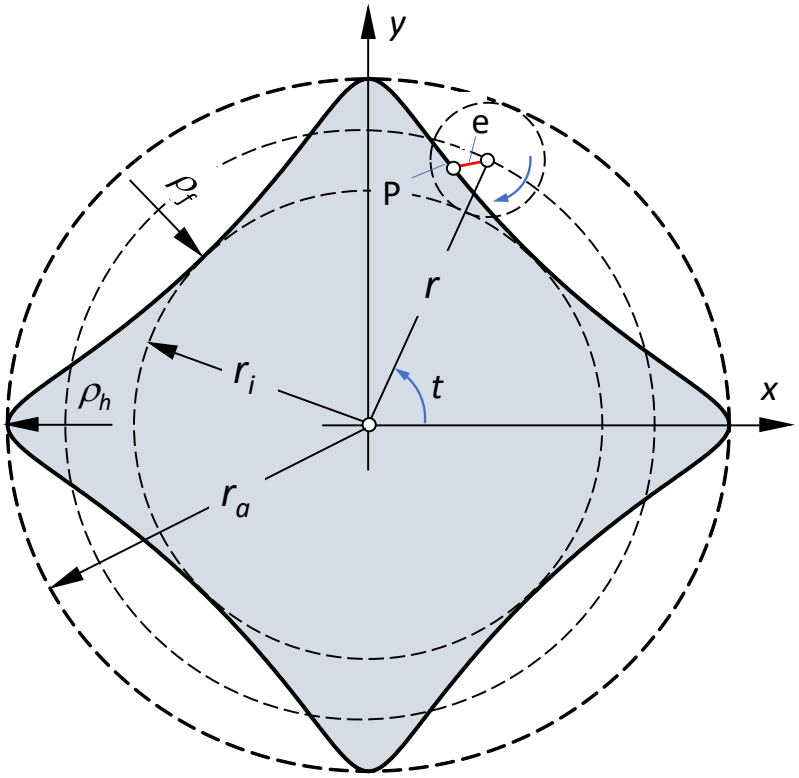

Figure 1. Description of hypotrochoid.

The diameter ratio defines the number of sides "*n*" and should be an integer to obtain a closed curve. The coordinates of the generated point P describe the parameter equations for the hypotrochoid (H-profile) as follows:

$$\boldsymbol{x(t) = r \cdot \cos(t) + e \cdot \cos[(n-1) \cdot t]}$$
$$\boldsymbol{y(t) = r \cdot \sin(t) - e \cdot \sin[(n-1) \cdot t]} \quad \text{with} \quad \boldsymbol{0^\circ \leq t \leq 360^\circ} \qquad (1)$$

The overlapping of the profile contour starts from the boundary eccentricities of $\boldsymbol{e_{grenz} = \frac{r}{n-1}}$ and $\boldsymbol{\varepsilon_{grenz} = \frac{1}{n-1}}$.

Figure 2 shows some examples of the H-profiles obtained for different numbers of sides (n) and eccentricities.

Preprints (www.preprints.org) | NOT PEER-REVIEWED | Posted: 16 December 2022 doi:10.20944/preprints202212.0289.v1

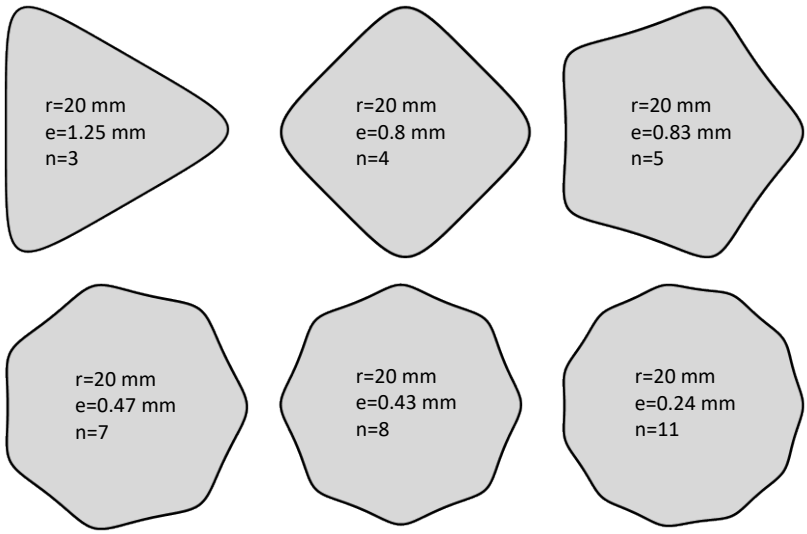

Figure 2. Examples of H-profiles with different numbers of sides (n) and eccentricities.

Geometric properties:

Area

Based on the principles for general trochoidal profiles described in [6], the geometric properties of the H-profiles were determined. Starting from the parameter representation (1) for the hypotrochoidal contours, the following complex mapping function is formulated as follows:

$$\boldsymbol{\omega(\zeta) = r \cdot \zeta + \frac{e}{\zeta^{n-1}}} \quad (2)$$

This mapping can conform to the contour of a profile to the perimeter of a unit circle. However, when the area enclosed by the polygon was mapped, multiple poles were formed at the corners of the contour.

Substituting the mapping in the following equation for the area ([8]), one obtains

$$\boldsymbol{A = \frac{1}{2}\int_0^{2\pi} Im[\bar{\omega}(\zeta) \cdot \dot{\omega}(\zeta)]\, dt} \quad (3)$$

The following relationship can be derived for the area enclosed by an H-profile for any number of drivers *n* and eccentricity *e:*

$$\boldsymbol{A = A_a - \pi \cdot e \cdot [d_a + e \cdot (n-2)]}, \quad (4)$$

where $\boldsymbol{\dot{\omega} = d\omega/dt}$ is the first derivative of the mapping function, t defines the parameter angle, and $\boldsymbol{A_a = \frac{\pi}{4} \cdot d_a^2}$ is the area of the head circle (with $\boldsymbol{d_a = 2 \cdot r_a}$).

Radius of curvature at profile corners

From a manufacturing point of view, the radius of the curvature of the contour at profile corners (on the head circle) plays an important role. Using the equation presented in [10],

$$\boldsymbol{\rho = 2i \cdot \frac{(\dot{\omega}\cdot\bar{\dot{\omega}})^{\frac{3}{2}}}{\bar{\omega}\cdot\ddot{\omega} - \dot{\omega}\cdot\bar{\ddot{\omega}}} = \frac{|\dot{\omega}|^3}{Im(\bar{\omega}\cdot\ddot{\omega})}} \quad (5)$$

The radius of curvature can be determined, and the second derivative of the mapping function is defined as $\boldsymbol{\ddot{\omega} = \frac{d^2\omega}{dt}}$.

Preprints (www.preprints.org) | NOT PEER-REVIEWED | Posted: 16 December 2022 doi:10.20944/preprints202212.0289.v1

The radius of curvature at profile corners (on the head circle in Figure 1) can be determined by substituting $t = 0$ in (5) as follows:

$$\boldsymbol{\rho_a} = \frac{(\boldsymbol{d_a}-2\cdot\boldsymbol{e}\cdot\boldsymbol{n})^2}{2\cdot[\boldsymbol{d_a}+2\cdot\boldsymbol{e}\cdot\boldsymbol{n}\cdot(\boldsymbol{n}-2)]} \tag{6}$$

The radius of curvature at profile corners is important in connection with the minimum tool diameter regarding the manufacturability of the profile.

The radius of curvature of the profile in the profile flank $\boldsymbol{\rho_f}$ (Figure 1) can also be determined using Equation (5) for $\boldsymbol{t} = \boldsymbol{\pi}/\boldsymbol{n}$:

$$\boldsymbol{\rho_f} = \frac{[\boldsymbol{d_a}+2\cdot\boldsymbol{e}\cdot(\boldsymbol{n}-2)]^2}{2\cdot[\boldsymbol{d_a}-2\cdot\boldsymbol{e}\cdot(\boldsymbol{n}^2-2\cdot\boldsymbol{n}+2)]}. \tag{7}$$

The radius of curvature in the flank area is a measure of the degree of the form fit of profile contours.

Bending stresses

The following elementary approach adopted from the literature was used to solve bending stresses [7]. It is assumed that the cross-sections remain as planes after loading. The following relationships are valid for the stresses

$$\begin{aligned}&\boldsymbol{\sigma_x} = \boldsymbol{\sigma_y} = \boldsymbol{\tau_{xy}} = \boldsymbol{\tau_{yz}} = \boldsymbol{\tau_{xz}} = \mathbf{0}\\ &\boldsymbol{\sigma_z} = -\frac{\boldsymbol{M_b}}{\boldsymbol{I_y}}\cdot\boldsymbol{x}\end{aligned} \tag{8}$$

where $\boldsymbol{I_y}$ denotes the moment of inertia for cross-sectional profiles relative to the y-axis (Figure 3).

Bending deformations

The displacements can be determined with the help of the corresponding consumptions and Hook's law. Based on this, the deflection is derived as follows:

$$\boldsymbol{u_x} = \frac{\boldsymbol{M_b}}{2\cdot\boldsymbol{E}\cdot\boldsymbol{I_y}}\cdot[\boldsymbol{z}^2 + \boldsymbol{\nu}\cdot(\boldsymbol{y}^2 - \boldsymbol{x}^2)] \tag{9}$$

Moments of inertia

The moment of inertia $\boldsymbol{I_y}$ is necessary for the calculation of the bending stress $\boldsymbol{\sigma_z}$ as well as for the determination of bending deformation $\boldsymbol{u_x}$ (Equations (8) and (9)).

The moment of inertia $\boldsymbol{I_y}$ involves a double integral over the profile's cross-section, but this can be reduced to a simple curvilinear integral over the profile contour using Green's theorem as follows:

$$\boldsymbol{I_y} = \frac{1}{3}\int_{\gamma}\boldsymbol{x}^3\boldsymbol{dy} \tag{10}$$

The contour description according to Equation (2) is also advantageous here. For the contour of the profile's cross-section, the following coordinates apply:

$$\begin{aligned}&\boldsymbol{x} = \frac{\boldsymbol{\omega(\lambda)} + \overline{\boldsymbol{\omega(\lambda)}}}{\mathbf{2}},\\ &\boldsymbol{y} = \frac{\boldsymbol{\omega(\lambda)}-\overline{\boldsymbol{\omega(\lambda)}}}{2\cdot\boldsymbol{i}}\end{aligned} \tag{11}$$

Substituting (11) in (10) $\boldsymbol{I_y}$ can be determined as follows:

$$\boldsymbol{I_y} = \frac{\boldsymbol{i}}{48}\int_{\gamma}\left(\boldsymbol{\omega(\lambda)} + \overline{\boldsymbol{\omega(\lambda)}}\right)^3\boldsymbol{d}\left(\boldsymbol{\omega(\lambda)} - \overline{\boldsymbol{\omega(\lambda)}}\right), \tag{12}$$

Preprints (www.preprints.org) | NOT PEER-REVIEWED | Posted: 16 December 2022 doi:10.20944/preprints202212.0289.v1

where $\boldsymbol{\lambda = e^{it}}$ takes. Function (12) facilitates the determination of the moment of inertia with the help of Equation (2).

Inserting the mapping function from (2) into Equations (12), the following relationship is determined for the bending moment of inertia for any number of flanks n and eccentricity e:

$$\boldsymbol{I_y = \frac{\pi}{4} \cdot \left(r^4 - 2e^2(n-2)r^2 - e^4(n-1) \right)} \quad (13)$$

If one substitutes x(t) from (1) and $\boldsymbol{I_y}$ from (13) into Equation (8), the distribution of the bending stress on the lateral surface of the profile can be determined as follows:

$$\boldsymbol{\sigma_b(t) = \frac{4M_b}{\pi} \cdot \frac{r\,cos(t) + e\,cos((n-1)t)}{r^4 - 2e^2(n-2)r^2 - e^4(n-1)}} \quad (14)$$

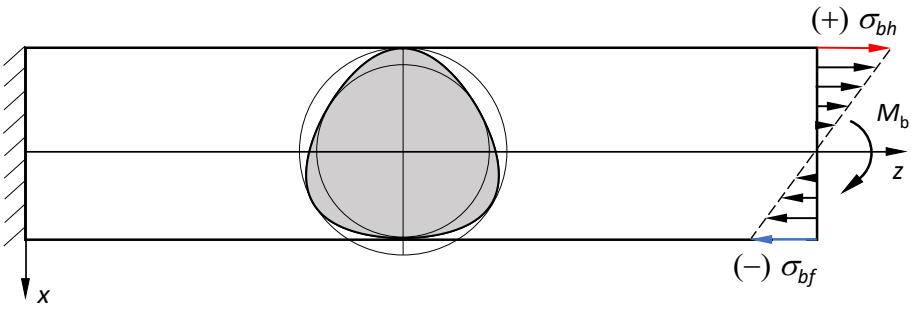

Figure 3. The bending coordinate system for a loaded profile shaft.

The maximum bending stress on the tension side occurs at $\boldsymbol{x = r + e}$ (on the profile head, Figure 3), and therefore the following equation applies:

$$\boldsymbol{\sigma_{bh} = \frac{4M_b}{\pi} \cdot \frac{r+e}{r^4 - 2e^2(n-2)r^2 - e^4(n-1)}} \quad (15)$$

The bending stress on the pressure side at $\boldsymbol{x = r - e}$ (in the middle of the profile flank on the foot circle, Figure 3) can also be determined as follows:

$$\boldsymbol{\sigma_{bf} = \frac{4M_b}{\pi} \cdot \frac{r-e}{r^4 - 2e^2(n-2)r^2 - e^4(n-1)}} \quad (16)$$

Example

In the following example, the analytical solution explained above is compared with the numerical and experimental results. An H-profile from DIN 3689-1 [4] with three sides, a head circle diameter of 40 mm with $\boldsymbol{r = 18.18}$ mm and $\boldsymbol{e = 1.818}$, (a related eccentricity $\boldsymbol{\varepsilon = 0.1}$ was chosen as the object of investigation. The bending load was chosen as $\boldsymbol{M_b}$= 500 Nm. Figure 4 shows the distribution of the bending stress on the circumference of the profile according to Equation (14) and its comparison with the numerical result. A good agreement between the results is observed.

Preprints (www.preprints.org) | NOT PEER-REVIEWED | Posted: 16 December 2022 doi:10.20944/preprints202212.0289.v1

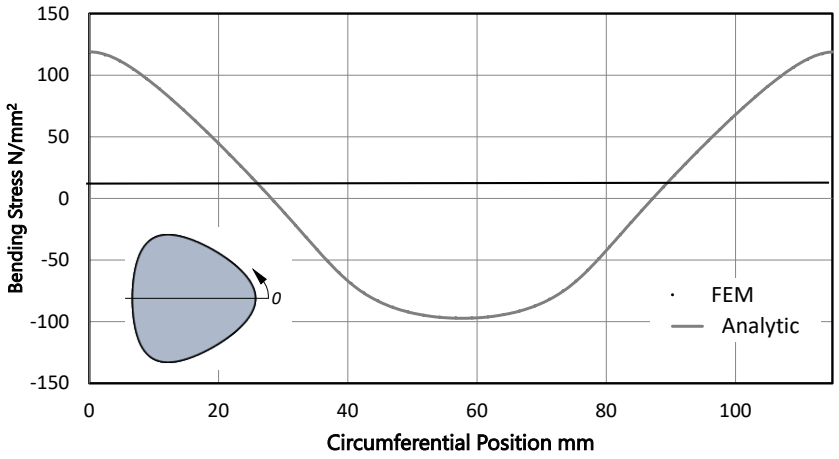

Figure 4. Circumferential distribution of the bending stress on the lateral surface of a standardised H3 profile.

In addition, bending stresses were experimentally determined for the head and foot areas and compared with Equations (15) and (16). Figure 5 also shows a very good agreement between the results.

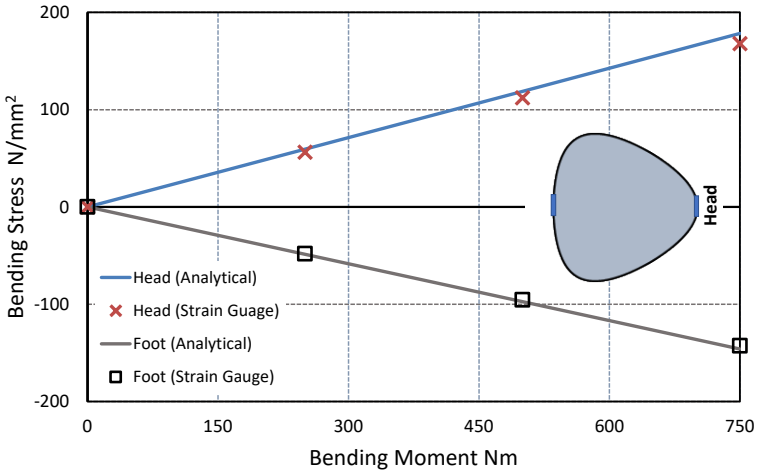

Figure 5. Comparison of the experimental results with the analytical solutions.

Stress factor for bending loads

The stress factor is defined as the ratio of the bending stress in a profile shaft to the corresponding reference stress for a round cross-section with radius *r*. For the head of the profile, the stress factor is determined as follows:

$$\alpha_{bh} = \frac{1+e}{1-2e^2(n-2)-e^4(n-1)} \tag{17}$$

Figure 6 shows the curves for the stress factor as a function of the relative eccentricity for different numbers of sides n. It can be seen from the figure that the stress factor in the profile shaft is the same as its reference stress. Figure 6 shows that the stress factor increases with an increase in eccentricity and the number of sides.

Preprints (www.preprints.org) | NOT PEER-REVIEWED | Posted: 16 December 2022 doi:10.20944/preprints202212.0289.v1

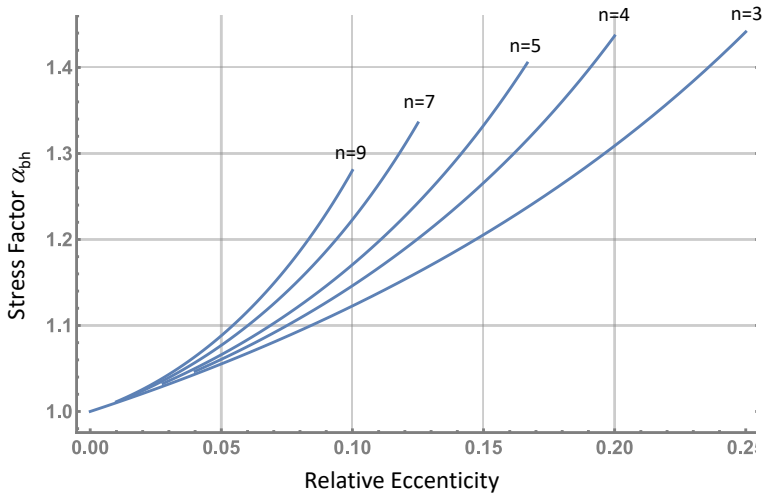

Figure 6. Stress factors for the bending stress at the profile head (Equation 15) with varying relative eccentricity and number of sides.

For the profile base (foot), the following stress factor is analogously obtained:

$$\boldsymbol{\alpha_{bf} = \frac{1-e}{1-2e^2(n-2)-e^4(n-1)}} \tag{18}$$

Rotating bending stress

Figure 7. schematically represents an H-profile with three flanks (according to DIN3689) in the Cartesian coordinates.

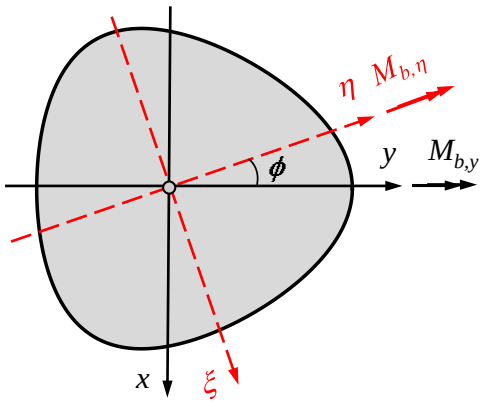

Figure 7. Rotated coordinate system for determining the bending moment of inertia.

Using the procedure described in [11], the following relationships are derived for $\boldsymbol{I_x}$ and $\boldsymbol{I_{xy}}$:

$$\boldsymbol{I_x = I_y}$$
$$\boldsymbol{I_{xy} = 0} \tag{19}$$

From Equations (19) and with the help of Mohr's circle, it can be proven that the moment of inertia is invariant and independent of the coordinate system (see also [6]):

$$\boldsymbol{I_\eta = I_y = I_x = \frac{\pi}{4} \cdot \left(r^4 - 2e^2(n-2)r^2 - e^4(n-1)\right)} \tag{20}$$

Preprints (www.preprints.org) | NOT PEER-REVIEWED | Posted: 16 December 2022 doi:10.20944/preprints202212.0289.v1

In order to obtain the general solution of the bending stress according to (8) for an arbitrary angle of rotation, the lever arm x is to be converted in the rotated coordinate system:

$$\boldsymbol{x_\phi = y\,cos(\phi) - x\,sin(\phi)}, \tag{21}$$

where phi denotes the angle of rotation. If the values for x and y from (1) are inserted into the relationship (14), the following equation results for the lever arm in the rotated coordinate system on the lateral surface ($\boldsymbol{0 \le t \le 2\pi}$):

$$\boldsymbol{x_\phi = r\,sin(t-\phi) - e\,sin\big((n-1)t+\phi\big)} \tag{22}$$

$$\boldsymbol{\sigma_b(\phi,t) = \frac{4M_b}{\pi} \cdot \frac{r\,sin(t-\phi) - e\,sin\big((n-1)t+\phi\big)}{r^4 - 2e^2(n-2)r^2 - e^4(n-1)}} \tag{23}$$

Figure 8 shows the distributions of the bending stresses on the profile contour for different angles of rotation, which were determined using Equation (23). As expected, the maximum stress occurred at the profile head.

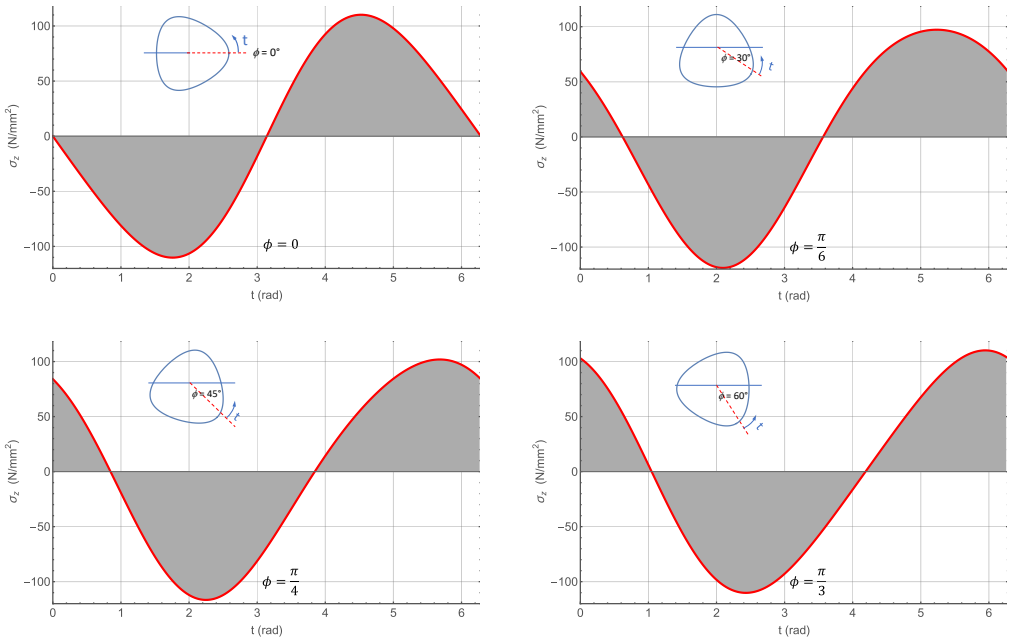

Figure 8. Distributions of the bending stresses on the profile contour for different angles of rotation.

Deflection

The deflection of the profile shaft can also be determined with the help of the bending moment of inertia $\boldsymbol{I_y}$. As explained in [6], and also above, this is independent of the angular position of the cross-section ϕ (Equation 23).

Displacements are determined using Hooke's law, and the corresponding correlation between displacements and the strain is determined as follows [5, 10]:

$$\boldsymbol{u_x = \frac{M_b}{2 \cdot E \cdot I_y} \cdot [z^2 + \nu \cdot (y^2 - x^2)]} \tag{24}$$

The deflection of the neutral axis is determined from $\boldsymbol{u_x}$ for $x = y = 0$ as follows:

$$\boldsymbol{\delta_x = \frac{M_b}{2 \cdot E \cdot I_y} \cdot z^2} \tag{25}$$

Substituting (20) in (25), the deflection can be determined as

Preprints (www.preprints.org) | NOT PEER-REVIEWED | Posted: 16 December 2022 doi:10.20944/preprints202212.0289.v1

$$\boldsymbol{\delta_x} = \frac{\boldsymbol{2M_b}}{\boldsymbol{\pi E}} \cdot \frac{\boldsymbol{z^2}}{\boldsymbol{r^4 - 2e^2(n-2)r^2 - e^4(n-1)}} \tag{26}$$

Example

Figure 9 shows the deflection for an H-section shaft with three flanks according to DIN3689-1 with a $\boldsymbol{d_a}$ = 40 mm (H3-40×32.73 with = 0.1) and a length of 160 mm made of steel (E=210000 $\frac{\boldsymbol{N}}{\boldsymbol{mm^2}}$). The comparison with FE analysis shows very good agreement with Equation (23), as can also be seen in Figure 10.

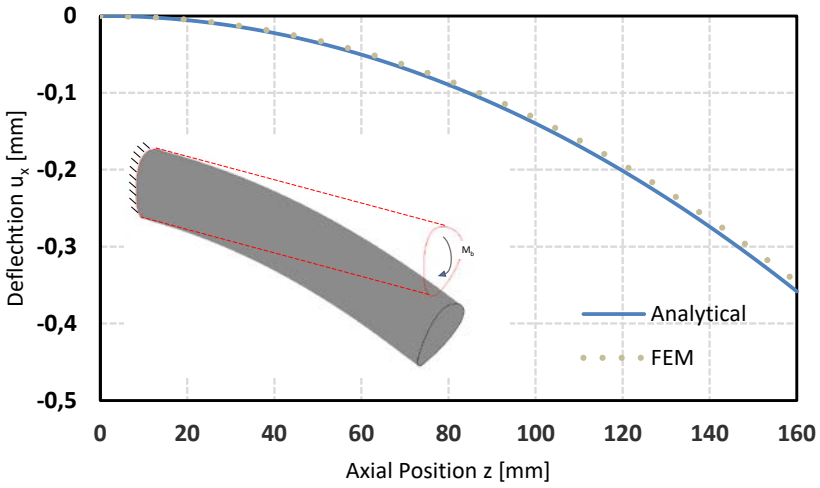

Figure 10. Deflection in a DIN3689-H3-40×32.73 profile.

H-profiles according to DIN3689-1

DIN3689-1 is a new standard that was published for the first time in December 2020. It describes the geometric properties of 18 specified H-profiles in 2 series. Series A is based on the head diameter, and series B involves the foot diameter as the nominal size of the profile. The respective corresponding profiles are geometrically similar. Each series contains 48 nominal sizes, which remain geometrically similar among themselves. Consequently, all standardised profiles are limited to 18 variants. This facilitates the processing of a generally valid design concept.

Stress factor for bending

The maximum bending stresses at the head and base of the profile are important from a technical point of view for the design of a profile shaft subject to bending. Therefore, in this section, the two stress factors $\boldsymbol{\alpha_{bh}}$ and $\boldsymbol{\alpha_{bf}}$ for all the 18 standard profile series were determined from Equations (18) and (19).

Stress factor for torsion

In [12], purely numerical investigations were carried out on the torsional stresses in H-section shafts. The analytical solution for torsion can be carried out using the approach of Muskhelishvili [7]. However, this requires a conformal mapping of the unit circle onto the polygon's cross-section. For H-sections, the mapping function derived from the parameters in Equation (1) cannot be directly used to solve the torsional stresses due to the multiple poles. The authors of [13] employ a complicated computational process to determine the polynomials required for the description of the mappings of H-profiles. In [5, 14, 15, 16], successive methods following Kantorovich [6] were used to develop a suitable mapping function in the form of a series converging to the profile contour. The convergence quality and limit were examined and presented depending on the number of terms

Preprints (www.preprints.org) | NOT PEER-REVIEWED | Posted: 16 December 2022 doi:10.20944/preprints202212.0289.v1

in the series developed in [5] for H-profiles calculating the torsional deformations for all standardised profiles. In the presented work, this method, accompanied by FEA, was used for all the 18 standardised profile geometries of DIN3689-1 to determine the maximum torsional stresses, which occur in the middle of the profile flank at the profile foot. A stress factor for torsional loading α_t was also determined analogously to that defined for the case of bending.

For practical applications, the results for the bending and torsional stress factors are compiled in Table 1. Using the relative eccentricity, no dependence on the shaft diameter occurs.

Table 1. Stress factors for bending and torsional loads for the H-profiles standardised according to DIN3689-1.

n	ε	α_{bh}	α_{bf}	I_y/I_0	α_t
3	0.100	1.12	0.92	0.980	1.23
4	0.056	1.07	0.96	0.988	1.17
	0.111	1.17	0.94	0.950	1.37
5	0.031	1.04	0.97	0.994	1.12
	0.063	1.09	0.96	0.977	1.24
	0.094	1.16	0.96	0.947	1.38
6	0.020	1.02	0.98	0.997	1.10
	0.040	1.05	0.97	0.987	1.19
	0.080	1.14	0.97	0.949	1.37
7	0.028	1.04	0.98	0.992	1.15
	0.056	1.09	0.97	0.969	1.29
	0.083	1.16	0.99	0.930	1.43
9	0.023	1.03	0.98	0.992	1.17
	0.047	1.08	0.98	0.969	1.31
	0.063	1.12	0.99	0.945	1.39
12	0.017	1.02	0.99	0.995	1.16
	0.033	1.06	0.99	0.978	1.28
	0.050	1.10	1.00	0.951	1.38

Table 1 lists the calculation results of the bending and torsional stress factors for all standardised profile geometries according to DIN3689-1 (rounded to two decimal places).

The bending moment of the inertia of a circular cross-section with radius r is defined as a reference moment of inertia and labelled I_0. The ratio between I_y and I_0 is also listed in Table 1 for the standardised profiles. The H-profiles are normally slightly more flexible than round profiles.

Conclusion

In this paper, an analytical approach was presented to determine the bending stresses and deformations in the hypotrochoidal profile shafts. Valid calculation equations for the area, radii of curvature of the profile contour, as well as the bending moment of inertia were derived for such profiles. Furthermore, the solutions for bending stresses and deformations were presented. For practical applications, a stress factor was defined for the critical locations on the profile contour.

The analytically determined results demonstrated very good agreement with both numerical and experimentally determined results.

The stress factors of the bending stresses were determined for all profile geometries standardised according to DIN3689-1, and the values obtained for practical applications

 doi:10.20944/preprints202212.0289.v1

were compiled in a table. Based on previous works of the author, the stress factors for torsional stresses were also determined and added to the table.

Acknowledgments: The author thanks the German Research Foundation (Deutsche Forschungsgemeinschaft DFG) for funding the research project DFG ZI 1161/2, which made this study possible.

Formula symbols:

A	mm²	Area of profile cross-section
e	mm	Profile eccentricity
e_{grenz}	mm	Profile overlap eccentricity limit
E	MPa	Young's modulus
n	-	Profile periodicity (number of sides)
I_0	mm⁴	Corresponding reference moments of inertia for a round cross-section with radius r
I_x, I_y, I_{xy}	mm⁴	Surface moments of inertia in the Cartesian coordinate system
$I_\xi, I_\eta, I_{\xi\eta}$	mm⁴	Surface moments of inertia in the rotated coordinate system
l	mm	Length of profile shaft
M_b	Nm	Bending moment
r	mm	Nominal or mean radius
t	-	Profile parameter angle
u_x	mm	Displacement in x direction
x, y, z	mm	Cartesian coordinates

Greek formula symbols:

α_{bh}	-	Bending stress factor for profile head
α_{bf}	-	Bending stress factor for profile foot
α_t	-	Torsional stress factor for profile head
δ_x	mm	deflection
$\varepsilon = e/r$	-	Relative eccentricity
ϕ	-	Rotation angle of the coordinate system
$\lambda = e^{i\theta}$	-	Physical plane unit circle
θ	-	Polar angle
σ_b, σ_z	MPa	Bending stress (z-component of stress vector)
τ_t	MPa	Torsional stress
$\omega(\zeta)$	-	Completed mapping function
$\omega_0(\zeta)$	-	Contour edge mapping function
ζ	-.	Complex variable in model plane
ξ, η	-	Coordinates in rotated system

References

1. Gold, P.W.: In acht Sekunden zum Polygon: wirtschaftliches Unrunddrehverfahren zur Herstellung von Polygon-Welle-Nabe-Verbindungen. Antriebstechnik, band 45, Heft 6, Seiten 42-22, 2006.
2. Stenzel, H. Unrunddrehen und Fügen zweiteiliger Getriebezahnräder mit polygonaler Welle-Nabe-Verbindungen, VDI-Berichte 2114, 4. Fachtagung Welle-Nabe-Verbindungen, Gestaltung Fertigung und Anwendung. Seiten 211-230, VDI-Verlag 2010.
3. Westsachsische Hochschule Zwickau, Ziaei, M. Patentanmeldung: Application of rolling processes using new reference profiles for the production of trochoidal inner and outer contours. DE 10 2019 000 654 A1, 2020.07.30
4. DIN 3689-1:2021-11, Welle-Nabe-Verbindung - Hypotrochoidische H-Profile - Teil 1: Geometrie und Maße. DIN-Deutsches Institut für Normung e.V.: Berlin, Germany, 2021.
5. Ziaei, M.: Torsionsspannungen in prismatischen, unrunden Profilwellen mit trochoidischen Konturen, Forschung im Ingenieurwesen, Ausgabe 4/2021.

6. Kantorovich, L.V.; Krylov, V.I.: Approximate Methods of Higher Analysis, Dover Publications, 2018.
7. Muskelishvili, N.I.: Some Basic Problems of the Mathematical Theory of Elasticity, Springer Dordrecht 1977.
8. Ziaei, M. Bending Stresses and Deformations in Prismatic Profiled Shafts with Noncircular Contours Based on Higher Hybrid Trochoids. Appl. Mech. 2022, 3, 1063-1079. https://doi.org/10.3390/applmech3030060.
9. Bronstein I. N. et al: Taschenbuch der Mathematik, 7th Auflage, Verlag Hari Deutsch, Frankfurt am Main, 2008.
10. Zwikker, C. The Advanced Geometry of Plane Curves and Their Applications, Dover Books on Advanced Mathematics, 1963.
11. Sokolnikoff, I.S.: Mathematical Theory of Elasticity. Robert E. Krieger Publishing Company, Malaba, Florida, 1983.
12. Schreiter, R.: Numerische Untersuchungen zu Form- und Kerbwirkungszahlen von hypotrochoidischen Polygonprofilen unter Torsionsbelastung, Dissertation TU Chemnitz, Chemnitz, 29.06.2022.
13. Ivanshin, P.N.; Shirokova E. A.: Approximate Conformal Mappings and Elasticity Theory, Journal of Complex Analysis, Hindawi Publishing Corporation, 2016, Article ID 4367205.
14. Ziaei, M.: Analytische Untersuchung unrunder Profilfamilien und numerische Optimierung genormter Polygonprofile für Welle-Nabe-Verbindungen „Habilitationsschrift“, Technische Universität Chemnitz, 2002.
15. Entwicklung eines analytischen Berechnungskonzeptes für formschlüssige Welle-Nabe-Verbindungen mit hypotrochoidischen Verbindungen, Abschlussbericht zum DFG-Vorhaben DFG ZI 1161/2 (Westsächsische Hochschule Zwickau) und LE 969/21(TU Chemnitz), Juli 2020.
16. Lee, K.: Mechanical Analysis of Fibers with a Hypotrochoidal Cross Section by Means of Conformal Mapping Function, Fibers and Polymers, Vol.11, No.4, 638-641, 2010